


ZnO-CuO Nanocomposite Synthesized by Co-precipitation: Characterization and Antibacterial Properties

Swapnali B. Dhage¹, Parvinder M. Sah², Jaya Lakkakula³, Rajesh W. Raut^{2,*}, Yuvraj S. Malghe^{1,*}, Arpita Roy^{4,*}, Devvret Verma⁵, Kirtanjot Kaur⁶

¹ Department of Chemistry, The Institute of Science, 15, Madam Cama Road, Dr. Homi Bhabha State University, 400032, Mumbai

² Department of Botany, The Institute of Science, 15, Madam Cama Road, Dr. Homi Bhabha State University, 400032, Mumbai

³ Centre for Computational Biology and Translational Research, Amity Institute of Biotechnology, Amity University Maharashtra Mumbai-Pune Expressway, Bhatan, Panvel, Mumbai, Maharashtra, 410206, India

⁴ Department of Biotechnology, Sharda School of Engineering & Technology, Sharda University, Greater Noida, India

⁵ Department of Biotechnology, Graphic Era Deemed to be University, Dehradun, Uttarakhand 248002, India

⁶ University Centre for Research & Development, Department of Chemistry, Chandigarh University, Gharuan, Mohali, Punjab, India

* Correspondence: rajesh.w.raut@gmail.com(R.W.R.), ymalghe@yahoo.com(Y.S.M.), arbt2014@gmail.com(A.R.);

Scopus Author ID 26327121200

Received: 7.08.2023; Accepted: 20.12.2023; Published: 4.02.2024

Abstract In this study, a nanocomposite was prepared using a co-precipitation method. TG-DTA, X-ray diffraction (XRD), Scanning electron micrograph (SEM-EDX), Fourier transform infrared spectroscopy (FTIR), Nanoparticle tracking analyzer (NTA), and UV-visible spectrometer analysis were used to characterize the as-prepared nanocomposite. From the XRD study, ZnO shows a hexagonal wurtzite structure, whereas CuO shows a monoclinic structure. UV-visible spectra indicate that a 3.20eV bandgap exists for the ZnO-CuO nanocomposite. The antibacterial activity of ZnO-CuO nanocomposite was evaluated using the Agar disk-diffusion method against *Staphylococcus aureus* (NCTC-8325), *Staphylococcus epidermidis* (ATCC-12228) (Gram-positive), *Salmonella typhi* (CT18), and *Escherichia coli* (ATCC-27853) (Gram-negative). A ZnO-CuO nanocomposite demonstrated effective antibacterial activity against the studied bacteria.

Keywords: ZnO-CuO nanocomposite; co-precipitation method; optical measurement; characterization; antibacterial study.

© 2024 by the authors. This article is an open-access article distributed under the terms and conditions of the Creative Commons Attribution (CC BY) license (<https://creativecommons.org/licenses/by/4.0/>).

1. Introduction

Nanotechnology, with its diverse properties, finds applications across various research domains, encompassing optical, mechanical, and electrical fields. The intricacies of nanotechnology are influenced by factors such as composition, size, and structural order, making it a versatile tool in various sectors. Beyond their role in energy production and efficiency, nanotechnology and nanoscience contribute significantly to agriculture, food industries, cosmetics, automotive technologies, medical advancements, drug development, computing, and household appliances [1]

Metal and metal oxide nanoparticles, including TiO₂ [2], ZnO [3], CuO [4], Ag [5], SnO₂ [6], and Fe₂O₃ [7], have been investigated for their antimicrobial properties against both

gram-positive and gram-negative strains [8]. Although these nanomaterials exhibit antibacterial activity individually, their effectiveness can be further heightened through synergistic interactions. Additionally, the photodynamic behavior of nanocomposites plays a pivotal role in augmenting antibacterial properties [1].

Nanocomposites, characterized by narrow size distributions and inherent non-dispersive, non-aggregative, and non-agglomerative qualities, are well-suited for various commercial applications [9]. Notably, ZnO, a typical n-type semiconductor with a direct bandgap of 3.24eV [10], and CuO, a p-type semiconductor with a bandgap of 1.4eV [11], offer unique semiconductor properties. The strategic combination of p-CuO and n-ZnO in heterojunctions leverages the advantages of p-n junctions [12]. This coupling in ZnO-CuO nanocomposites substantially reduces the electron-hole pair recombination rate, facilitating effective charge carrier separation and transforming it into a visible light-active material [13]. Such properties suggest a potential for higher photodynamic antibacterial activities in ZnO-CuO nanocomposites.

This study details a method for developing ZnO-CuO nanocomposites through co-precipitation. Employing the Agar disk-diffusion method [13], we systematically examined the antibacterial efficacy of ZnO-CuO nanocomposites against *Staphylococcus aureus* (NCTC-8325), *Staphylococcus epidermidis* (ATCC-12228), *Salmonella typhi* (CT18), and *Escherichia coli* (ATCC-27853). The nanocomposites, prepared and annealed, underwent a comprehensive characterization utilizing diverse techniques, ensuring a thorough understanding of their structural and functional attributes.

2. Materials and Methods

2.1. Sample preparation.

ZnO-CuO composites were prepared using the co-precipitation method. 0.1M ZnCl₂ dry solution was slowly added to 0.1M CuCl₂.2H₂O solution while stirring constantly. The pH of the solution was maintained at 12 by adding NaOH. As-prepared nanocomposites were washed several times with deionized water and filtered through Whatman filter paper No. 41 to obtain ZnO-CuO composite precipitate. The precipitate was dried at 80°C for four hours. After preparing the composite, they were calcined at 600°C, 700°C, and 800°C for 3 hours.

2.2. Characterization.

TG-DTA curves of ZnO-CuO nanocomposites were recorded using the TG/DTA system (Rigaku, model Thermo Plus TG8120). An X-ray diffractometer (Rigaku, Model-Miniflex II) was used to record the XRD using monochromatic CuK α radiation ($k = 0.15405\text{nm}$) at a scan rate of 2 degrees $2\theta \text{ min}^{-1}$. The Perkin-Elmer spectrometer was used to record FTIR spectra. NTA LM20 nanoparticle tracking analyzer system (Nanosight Limited, Amesbury, UK) was used to measure particle size. Shimadzu (Model-1900i) recorded the UV-visible absorbance spectrum. Using SEM (JEOL-JSM6360A), the ZnO-CuO nanocomposite microstructure was analyzed.

2.3. Antibacterial activity.

The antimicrobial potential of the ZnO-CuO composite was investigated against both gram-negative bacteria, including *Salmonella typhi* (CT18) and *Escherichia coli* (ATCC-

27853), as well as gram-positive bacteria, namely *Staphylococcus aureus* (NCTC-8325) and *Staphylococcus epidermidis* (ATCC-12228). The Agar disk-diffusion method, a widely recognized technique for evaluating antimicrobial activity, was employed for this study [14].

To initiate the experiments, a 24-hour culture of the aforementioned microorganisms was prepared in nutrient broth. Subsequently, 50 μ l of the microbial inoculum was evenly spread onto each sterile Petri dish using a spreader within the laminar airflow chamber during the agar plate culture experiments. The turbidity standard utilized for the microbial culture was set at 0.5 McFarland, equivalent to 1–2 x 10⁸CFU/ml [15]. Four ZnO-CuO composite discs (6 mm in diameter) were prepared for the antimicrobial assay, each containing varying concentrations of the composite material (5mg/ml, 10mg/ml, 15mg/ml, and 20mg/ml). Additionally, a standard antibiotic disk containing ampicillin (positive control) was included in the setup. These discs were carefully placed on the surface of the inoculated nutrient broth agar plate using sterile forceps, ensuring complete contact with the agar surface. The plates were then incubated at 37°C.

After incubation, an examination of the plates revealed the presence of inhibition zones around each disc. The size of these inhibition zones served as an indicator of the efficacy of the ZnO-CuO composite against the tested microorganisms. Each disc's effectiveness was evaluated by measuring the diameter of the inhibition zone surrounding it. This methodology allowed for a comprehensive assessment of the antimicrobial activity of the ZnO-CuO composite across different concentrations, providing valuable insights into its potential as an effective agent against both gram-negative and gram-positive bacteria. The inclusion of a standard antibiotic control further facilitated the comparison of the composite's performance, contributing to a robust evaluation of its antimicrobial efficacy.

3. Results and Discussion

3.1. TG and DTA study.

The TG-DTA analysis was performed to determine the ZnO-CuO nanocomposite's calcination temperature and weight loss. Figure 1 depicts the TG and DTA curves of the ZnO-CuO nanocomposite as prepared under nitrogen at a heating rate of 10°C min⁻¹. Continuous weight loss was observed up to 560°C on the TG curve. There was no weight loss beyond 600°C. 19% of the weight was lost when heated up to 560°C. Two endothermic peaks were observed on the DTA curve, one at 180°C due to water loss and a second at 290°C due to inorganic material loss. TG and DTA curves indicate that ZnO-CuO nanocomposite can be formed around 600°C. Therefore, the prepared powders were calcined at 600°C for 3 hours to obtain the final product.

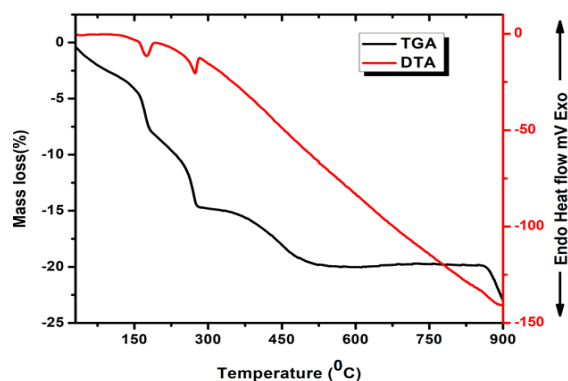


Figure 1. TG and DTA curves of a precursor.

3.2. XRD study.

XRD patterns for all the samples are almost identical, with intense peaks indicating the crystallinity of the materials. XRD peaks appeared at 2θ values of 31.90, 34.50, 36.45, 47.50, 56.71, 62.89, 66.25, 67.97, and 69.27, corresponding to the ZnO crystal planes (100), (002), (101), (102), (021), (103), (200), (112), (201) respectively. Similarly, XRD peaks appeared at 2θ values of 35.57, 38.83, 48.80, 58.55, and 61.69, corresponding to CuO crystal planes (-111), (111), (-202), (202), (-113), (103), (201), respectively. All diffraction peaks were in good agreement with the hexagonal wurtzite phase of ZnO (JCPDS No. 36-1451) [16] and Monoclinic CuO (JCPDS No. 48-1548) structure [17]. Figure 2 exhibits XRD patterns of ZnO-CuO nanocomposite annealed at 600°C, 700°C, and 800°C for 3 h in the scan range from 200 to 800.

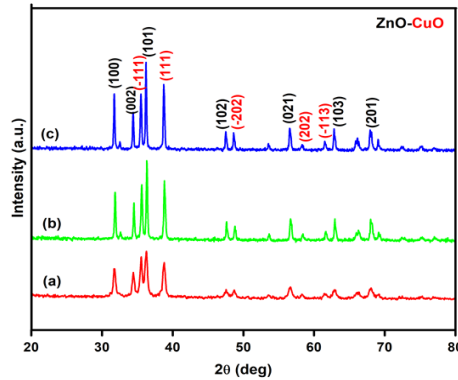


Figure 2. XRD pattern of the nanocomposite.

3.3. FT-IR study.

The FTIR spectrum of ZnO-CuO nanocomposite is shown in Figure 3. The ZnO-CuO nanocomposite exhibited sharp and well-defined peaks at 432.05, 471.36, 524.64, 542.86, 594.06, 1483.26, and 3318 cm^{-1} . The peaks at 432.05 cm^{-1} and 471.36 cm^{-1} may correspond to Zn-O stretching vibration bonds [18]. A Cu-O vibration may be responsible for the absorption peaks at 524.64 cm^{-1} and 594.06 cm^{-1} [19]. The vibration modes of Zn-O bonds may cause the vibration peak at 1438.26 cm^{-1} . The -OH moisture group in the sample is likely responsible for the small absorption peak at 3318 cm^{-1} .

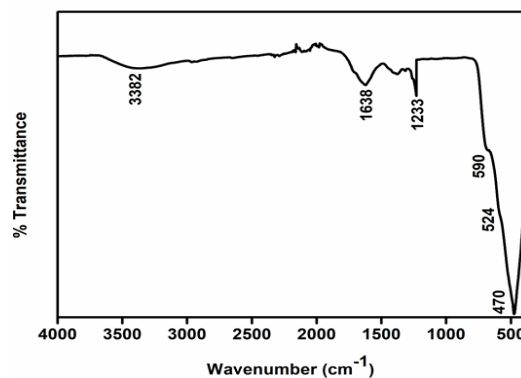


Figure 3. FT-IR spectra of the nanocomposite.

3.4. UV-visible study.

ZnO exhibits distinct n-type semiconductor characteristics, characterized by a direct bandgap of 3.24eV [10], while CuO functions as a p-type semiconductor with a bandgap of 1.4eV [11]. The intentional amalgamation of p-CuO and n-ZnO in heterojunctions strategically leverages the intrinsic advantages of p-n junctions [12]. This synergistic integration within

ZnO-CuO nanocomposites substantially mitigates the rate of electron-hole pair recombination. Consequently, this process facilitates the efficient separation of charge carriers, transforming the nanocomposite into a material highly responsive to visible light [13].

The formation of the nanocomposite, coupled with the existence of surface-related defects in the nanoparticles, results in a broad absorption spectrum. This phenomenon significantly influences optical parameters, including the complex refractive index and absorption coefficient, thereby enhancing the nanomaterial's properties. The inset of the Tauc plot of the ZnO-CuO nanocomposite is presented for reference. Tauc plots were employed to ascertain the bandgap of the ZnO-CuO nanocomposite, which was determined to be 3.2 eV [20]. The introduction of CuO induces a redshift in the bandgap of ZnO. Figure 4 visually depicts the UV-visible absorbance spectrum of the ZnO-CuO nanocomposite after heat treatment at 600°C.

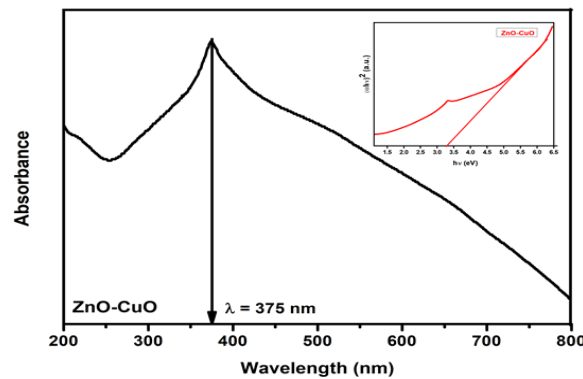


Figure 4. UV-Visible absorbance spectra of nanocomposite.

3.5. SEM and EDX study.

The application of scanning electron microscopy (SEM) played a pivotal role in unraveling the intricacies of the Cu-Zn material properties, particularly when subjected to a calcination process at 600°C, as elucidated in Figure 6. The SEM images provided unequivocal evidence that ZnO and CuO manifest heterogeneously, forming a distinctive nanocomposite structure. At this elevated temperature, ZnO nanoparticles intricately intertwine with CuO nanoparticles, creating a composite material with unique morphological characteristics.

In the realm of elemental composition analysis, SEMs offer a powerful tool when coupled with energy-dispersive X-ray (EDX) spectroscopy. Figure 5 showcases the ZnO-CuO nanocomposite's EDX pattern, revealing insights into the elemental constituents. The spectrum exhibits sharp peaks corresponding to Zinc, Copper, and Oxygen. Remarkably, no other peaks are discernible within the detection limit, affirming the exclusive composition of the synthesized materials, consisting solely of Zinc, Copper, and Oxygen.

Furthermore, the quantitative elemental analysis derived from the EDX data provides a detailed breakdown of the nanocomposite's composition. The ZnO-CuO nanocomposite, as revealed by the EDX pattern, boasts a zinc content of 37.38%, a copper content of 41.89%, and an oxygen content of 20.73%. This thorough elemental breakdown not only underscores the accuracy and precision of SEM-EDX analysis but also provides valuable information about the stoichiometry of the synthesized nanocomposite.

Beyond surface composition, the SEM-EDX approach also facilitates a depth analysis, unraveling the spatial distribution of elements within the nanocomposite structure. This depth profiling is particularly advantageous in discerning the intricate interplay and distribution of

Zinc, Copper, and Oxygen throughout the material, shedding light on the homogeneity and structural integrity of the synthesized Cu-Zn nanocomposite.

In essence, the integration of SEM imaging with EDX analysis validates the heterogeneous formation of ZnO and CuO within the nanocomposite and offers a comprehensive understanding of its elemental composition and distribution. This robust analytical approach stands as a cornerstone in unraveling the material intricacies and guiding the optimization of Cu-Zn nanocomposites for various applications.

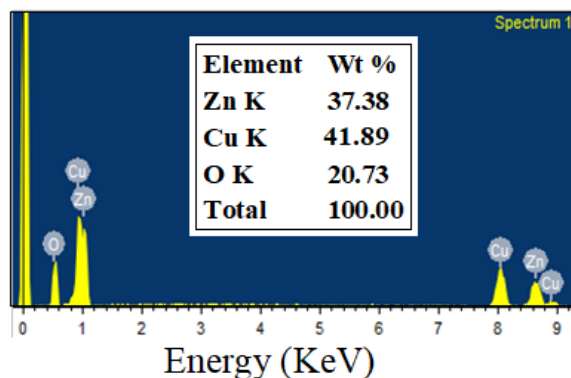


Figure 5. EDX analysis of the nanocomposite.

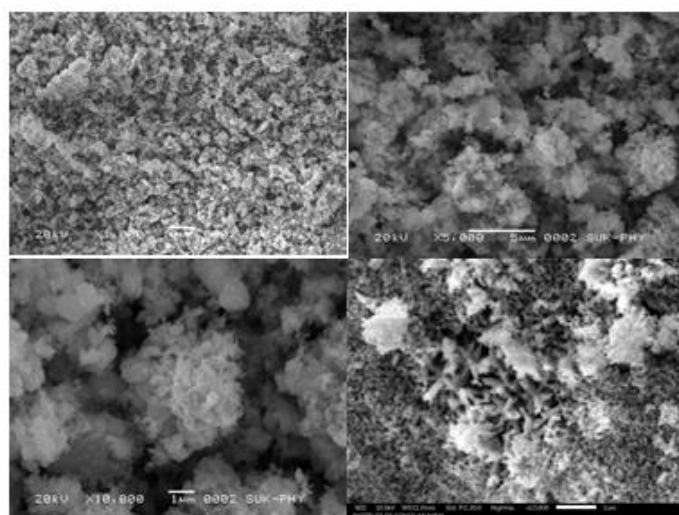


Figure 6. SEM image of the nanocomposite.

3.6. Particle size distribution study.

The determination of particle size distribution for ZnO-CuO powder involved employing nanoparticle tracking analysis (NTA). The nanomaterial was dispersed in distilled water and subjected to one minute sonication to ensure proper suspension. The particle size distribution for ZnO-CuO precursors, following a three-hour calcination process at 600°C, is depicted in Figure 7. According to the nanoparticle tracking analysis conducted in our study, ZnO-CuO at 600°C exhibits an average particle size of 51nm. The particle size distribution curve illustrates that the maximum number of particles in this nanomaterial cluster is around 51nm in size. This precise characterization through NTA provides valuable insights into the size distribution and dispersity of ZnO-CuO nanoparticles, essential considerations for understanding their behavior and potential applications in various fields.

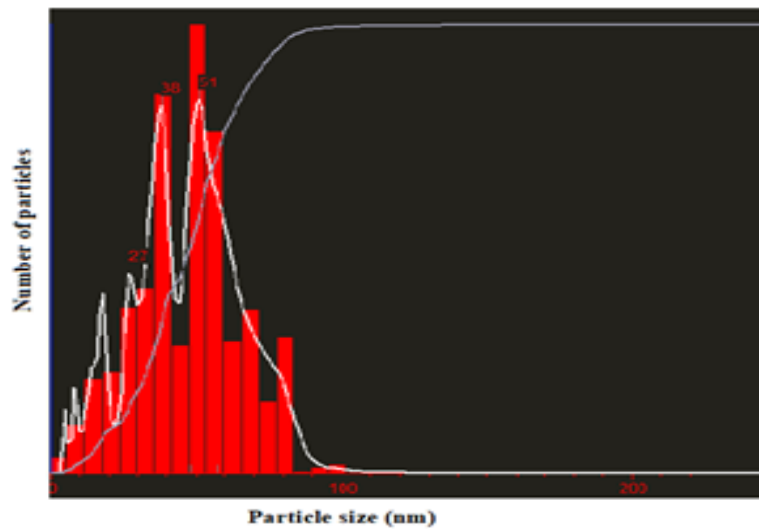


Figure 7. Particle size distribution curve for nanocomposite.

3.7. Antibacterial activity.

Exploring antibacterial agents combating bacterial resistance has become a focal point in research and development. Figure 8 illustrates the antibacterial efficacy of ZnO-CuO nanocomposite materials against *Salmonella typhi* (CT18), *Escherichia coli* (ATCC-27853) (Gram-negative), and *Staphylococcus aureus* (NCTC-8325), as well as *Staphylococcus epidermidis* (ATCC-12228) (Gram-positive).

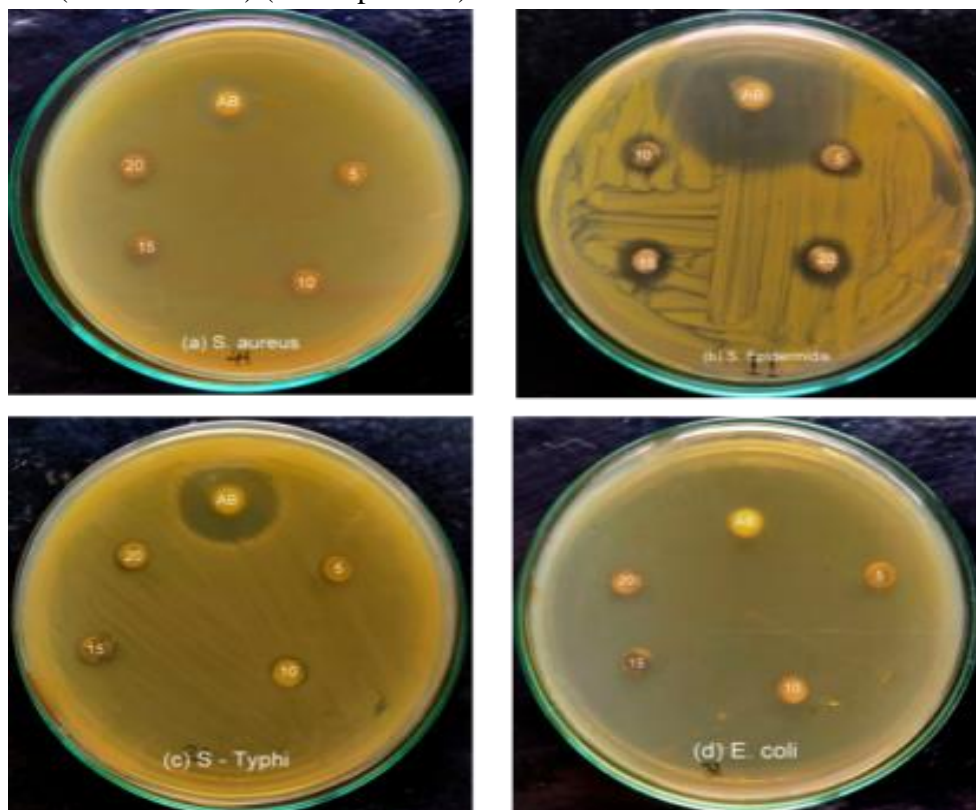


Figure 8. Antimicrobial activity of CuO-ZnO nanocomposite against (a) *Staphylococcus aureus*; (b) *Staphylococcus epidermidis*; (c) *Salmonella typhi*; (d) *Escherichia coli*.

The study discerned a notable increase in the zone of inhibition at higher concentrations of the nanocomposite colloid. Tiwari *et al.* [21] observed that exposure of bacteria to ZnO nanoparticles led to the production of reactive oxygen species (ROS), causing membrane lipid

peroxidation and subsequent leakage of sugars, proteins, and DNA across the membrane, ultimately resulting in bacterial death. Likewise, Meghana *et al.* [22] proposed that the antibacterial effect of CuO nanoparticles was attributed to ROS generation. Tariq *et al.* [23] highlighted the superior antibacterial activity of ZnO-CuO nanocomposite compared to pristine ZnO. They suggested that oxidative stress, induced by the electron transfer pathway and ROS, was responsible for the biocidal activity. Notably, in the current investigation, the nanocomposite exhibited enhanced antibacterial activity against Gram-positive bacteria compared to Gram-negative bacteria.

The band gap analysis in this study indicates a lower electron-hole pair recombination rate and higher defect density [23], rendering the ZnO-CuO nanocomposite a visible light-active material. This phenomenon plays a crucial role in the observed antibacterial activity of the nanocomposite.

Table 1. The measurement of the zone of inhibition for antibacterial strains.

Bacterial Strains	Ampicillin	ZC 5	ZC 10	ZC 15	ZC 20
	Zone of Inhibition (ZOI) in mm				
<i>S. aureus</i> (NCTC-8325)	17	10	12	14	15
<i>S. epidermidis</i> (ATCC-12228)	50	10	11	12	13
<i>S. typhi</i> (CT18)	23	7	9	11	12
<i>E. coli</i> (ATCC-27853)	9	8	10	12	14

4. Conclusions

Co-precipitation was used in this study to prepare a nanocomposite. ZnO-CuO nanocomposites were obtained. The composite nanoparticles were measured to be 51 nm in size. The ZnO component of the composite displays a hexagonal wurtzite structure, whereas the CuO component exhibits a monoclinic structure. Flakes and rods make up the morphology of the nanocomposite. The percentage concentration of Zn, Cu, and O in the nanocomposite was 37.38, 41.89, and 20.73, respectively. The bandgap was determined to be 3.20eV, suggesting a low electron-hole pair recombination rate. Also, the defect density was higher, which makes the material a visible light active material. Consequently, the nanocomposite has better antibacterial properties. A 20% concentration of nanocomposite showed maximum activity against gram-positive bacteria.

Funding

The full paper was self-funded.

Acknowledgments

The authors would like to thank their university for providing support to complete this work.

Conflicts of Interest

The author has no conflict of interest.

References

1. Harish, V.; Tewari, D.; Gaur, M.; Yadav, A.B.; Swaroop, S.; Bechelany, M.; Barhoum, A. Review on Nanoparticles and Nanostructured Materials: Bioimaging, Biosensing, Drug Delivery, Tissue Engineering,

- Antimicrobial, and Agro-Food Applications. *Nanomaterials* **2022**, *12*, 457, <https://doi.org/10.3390/nano12030457>.
2. Sukhadeve, G.K.; Bandewar, H.; Janbandhu, S.Y.; Jayaramaiah, J.R.; Gedam, R.S. Photocatalytic hydrogen production, dye degradation, and antimicrobial activity by Ag-Fe co-doped TiO₂ nanoparticles. *J. Mol. Liq.* **2023**, *369*, 120948, <https://doi.org/10.1016/j.molliq.2022.120948>.
 3. Abdelghany, T.M.; Al-Rajhi, A.M.H.; Yahya, R.; Bakri, M.M.; Al Abboud, M.A.; Yahya, R.; Qanash, H.; Bazaid, A.S.; Salem, S.S. Phytofabrication of zinc oxide nanoparticles with advanced characterization and its antioxidant, anticancer, and antimicrobial activity against pathogenic microorganisms. *Biomass Conv. Bioref.* **2023**, *13*, 417–430, <https://doi.org/10.1007/s13399-022-03412-1>.
 4. Ahamed, M.; Alhadlaq, H.A.; Khan, M.A.M.; Karuppiyah, P.; Al-Dhabi, N.A. Synthesis, Characterization, and Antimicrobial Activity of Copper Oxide Nanoparticles. **2014**, *2014*, 637858, <https://doi.org/10.1155/2014/637858>.
 5. Franzolin, M.R.; Courrol, D.d.S.; Silva, F.R.d.O.; Courrol, L.C. Antimicrobial Activity of Silver and Gold Nanoparticles Prepared by Photoreduction Process with Leaves and Fruit Extracts of *Plinia cauliflora* and *Punica granatum*. *Molecules* **2022**, *27*, 6860, <https://doi.org/10.3390/molecules27206860>.
 6. Obeizi, Z.; Benbouzid, H.; Bouarroudj, T.; Benzaid, C.; Djahoudi, A. Synthesis, characterization of (Ag-SnO₂) nanoparticles and investigation of its antibacterial and anti-biofilm activities. *J. New Technol. Mater.* **2020**, *10*, 10–17, <https://doi.org/10.12816/0058531>.
 7. Das, D.; Ali, S.; Rajbanshi, B.; Ray, S.; Barman, S.; Chouhan, D.; Haydar, M.S.; Mandal, P.; Roy, K.; Dakua, V.K.; Nath Roy, M. Synthesis of Biogenic Hematite Nanocubes as Recyclable Dark Fenton-like Catalysts at Neutral pH and Plant Growth Applications of Degraded Waste Water. *ACS Omega* **2022**, *7*, 44698–44710, <https://doi.org/10.1021/acsomega.2c03798>.
 8. Gold, K.; Slay, B.; Knackstedt, M.; Gaharwar, A.K. Antimicrobial Activity of Metal and Metal-Oxide Based Nanoparticles. *Adv. Ther.* **2018**, *1*, 1700033, <https://doi.org/10.1002/adtp.201700033>.
 9. Raza, S.; Ansari, A.; Siddiqui, N.N.; Ibrahim, F.; Abro, M.I.; Aman, A. Biosynthesis of silver nanoparticles for the fabrication of non cytotoxic and antibacterial metallic polymer based nanocomposite system. *Sci. Rep.* **2021**, *11*, 10500, <https://doi.org/10.1038/s41598-021-90016-w>.
 10. Sáenz-Trevizo, A.; Amézaga-Madrid, P.; Pizá-Ruiz, P.; Antúnez-Flores, W.; Miki-Yoshida, M. Optical Band Gap Estimation of ZnO Nanorods. *Mat. Res.* **2016**, *19*, 33–38, <https://doi.org/10.1590/1980-5373-MR-2015-0612>.
 11. Izaki, M.; Abe, S.; Nakakita, K.; Khoo, P.L. Photoelectrochemically Fabricated and Heated Cu₂O/CuO Bilayers with Enhanced Photovoltaic Characteristics. *ACS Omega* **2021**, *6*, 27587–27597, <https://doi.org/10.1021/acsomega.1c05163>.
 12. Lim, Y.-F.; Choi, J.J.; Hanrath, T. Facile Synthesis of Colloidal CuO Nanocrystals for Light-Harvesting Applications. *J. Nanomater.* **2012**, *2012*, 393160, <https://doi.org/10.1155/2012/393160>.
 13. Yoo, R.; Yoo, S.; Lee, D.; Kim, J.; Cho, S.; Lee, W. Highly selective detection of dimethyl methylphosphonate (DMMP) using CuO nanoparticles/ZnO flowers heterojunction. *Sens. Actuators B Chem.* **2017**, *240*, 1099–1105, <https://doi.org/10.1016/j.snb.2016.09.028>.
 14. Dhanasegaran, K.; Djearmane, S.; Liang, S.X.T.; Wong, L.S.; Kasivelu, G.; Lee, P.F.; Lim, Y.M. Antibacterial properties of zinc oxide nanoparticles on *Pseudomonas aeruginosa* (ATCC 27853). *Sci. Iran.* **2021**, *28*, 3806–3815.
 15. Hossain, M.L.; Lim, L.Y.; Hammer, K.; Hettiarachchi, D.; Locher, C. A Review of Commonly Used Methodologies for Assessing the Antibacterial Activity of Honey and Honey Products. *Antibiotics* **2022**, *11*, 975, <https://doi.org/10.3390/antibiotics11070975>.
 16. Basnet, P.; Samanta, D.; Inakhunbi Chanu, T.; Mukherjee, J.; Chatterjee, S. Assessment of synthesis approaches for tuning the photocatalytic property of ZnO nanoparticles. *SN Appl. Sci.* **2019**, *1*, 633, <https://doi.org/10.1007/s42452-019-0642-x>.
 17. Basaleh, A.S. Construction of mesoporous ZnFe₂O₄-g-C₃N₄ nanocomposites for enhanced photocatalytic degradation of acridine orange dye under visible light illumination adopting soft- and hard-template-assisted routines. *J. Mater. Res. Technol.* **2021**, *11*, 1260–1271, <https://doi.org/10.1016/j.jmrt.2021.01.110>.
 18. Kandi, V.; Kandi, S. Antimicrobial properties of nanomolecules: potential candidates as antibiotics in the era of multi-drug resistance. *Epidemiol. Health* **2015**, *37*, e2015020, <https://doi.org/10.4178/epih/e2015020>.
 19. Karthik, K.; Jaya, V.N.; Kanagaraj, M.; Arumugam, S. Temperature-dependent magnetic anomalies of CuO nanoparticles. *Solid State Commun.* **2011**, *151*, 564–568, <https://doi.org/10.1016/j.ssc.2011.01.008>.

20. T. Ranjan, L. Durgamadhab, M. Arindam, and B. Editors, "Lecture Notes in Electrical Engineering 781 Micro and Nanoelectronics Devices, Circuits and Systems Select Proceedings of MNDCS 2021," 2021, [Online]. Available: <http://www.springer.com/series/7818>.
21. Djearamane, S.; Loh, Z.C.; Lee, J.J.; Wong, L.S.; Rajamani, R.; Luque, P.A.; Gupta, P.K.; Liang, S.X.T. Remedial Aspect of Zinc Oxide Nanoparticles Against *Serratia Marcescens* and *Enterococcus Faecalis*. *Front. Pharmacol.* **2022**, *13*, 891304, <https://doi.org/10.3389/fphar.2022.891304>.
22. Fan, X.; Yahia, L.; Sacher, E. Antimicrobial Properties of the Ag, Cu Nanoparticle System. *Biology* **2021**, *10*, 137, <https://doi.org/10.3390/biology10020137>.
23. Jan, T.; Azmat, S.; Mansoor, Q.; Waqas, H.M.; Adil, M.; Ilyas, S.Z.; Ahmad, I.; Ismail, M. Superior antibacterial activity of ZnO-CuO nanocomposite synthesized by a chemical Co-precipitation approach. *Microb. Pathog.* **2019**, *134*, 103579, <https://doi.org/10.1016/j.micpath.2019.103579>.